

# Efficient and Scalable Monocular Human-Object Interaction Motion Reconstruction

Boran Wen<sup>1,2\*</sup> Ye Lu<sup>1\*</sup> Keyan Wan<sup>3</sup> Sirui Wang<sup>4</sup> Jiahong Zhou<sup>1</sup> Junxuan Liang<sup>1,2</sup>  
Xinpeng Liu<sup>1,2</sup> Bang Xiao<sup>1</sup> Dingbang Huang<sup>1</sup> Ruiyang Liu<sup>5</sup> Yong-Lu Li<sup>1,2†</sup>

<sup>1</sup>SJTU, <sup>2</sup>SII, <sup>3</sup>FDU, <sup>4</sup>BJTU, <sup>5</sup>STU

## Abstract

Generalized robots must learn from diverse, large-scale human-object interactions (HOI) to operate robustly in the real world. Monocular internet videos offer a nearly limitless and readily available source of data, capturing an unparalleled diversity of human activities, objects, and environments. However, accurately and scalably extracting 4D interaction data from these in-the-wild videos remains a significant and unsolved challenge. Thus, in this work, we introduce **4DHOISolver**, a novel and efficient optimization framework that constrains the ill-posed 4D HOI reconstruction problem by leveraging sparse, human-in-the-loop contact point annotations, while maintaining high spatio-temporal coherence and physical plausibility. Leveraging this framework, we introduce **Open4DHOI**, a new large-scale 4D HOI dataset featuring a diverse catalog of **144** object types and **103** actions. Furthermore, we demonstrate the effectiveness of our reconstructions by enabling an RL-based agent to imitate the recovered motions. However, a comprehensive benchmark of existing 3D foundation models indicates that automatically predicting precise human-object contact correspondences remains an unsolved problem, underscoring the immediate necessity of our human-in-the-loop strategy while posing an open challenge to the community. Data and code will be publicly available at <https://wenboran2002.github.io/open4dhoi/>

## 1. Introduction

The quest for generalized robot systems, capable of understanding and interacting with the complex real world, fundamentally relies on rich, high-fidelity 4D (3D + time) human-object interaction (HOI) data. This data is invaluable for providing crucial insights into human motor skills, intent, and physical reasoning, empowering applications to train intelligent robotic agents for dexterous manipulation to populating virtual worlds with realistic digital humans for gaming and VR/AR applications.

Despite its importance, acquiring generalized 4D HOI data remains a significant challenge. Existing multi-sensor oriented HOI capture systems, exemplified by BEHAVE [2], offer high-precision reconstructions by leveraging multi-view camera setups and sophisticated sensor arrays. However, the associated cost, from numerous cameras, sensors, and specialized studios, is prohibitive for large-scale data collection. Consequently, these systems are often confined to controlled indoor settings with limited object diversity, preventing the capture of HOI data for common outdoor activities like riding and surfing, as well as complex on-site construction tasks involved in industrial manufacturing processes.

Recognizing the limitations of high-precision capture systems, recent research has explored reconstructing 3D HOI from widely available monocular images. For example, Open3DHOI [35] relies on manual object pose adjustment in Blender, while PICO [6] proposes annotating contact regions. However, while effective for static images, both annotation strategies become prohibitively expensive and time-consuming when applied to video sequences, and they fundamentally struggle to enforce spatio-temporal consistency across frames. To address these critical challenges, we propose **4DHOISolver**, a novel and efficient framework for generating high-quality, temporally-consistent 4D HOI data from diverse monocular internet videos.

Our core idea is to replace expensive, dense labeling with a lightweight and efficient coarse contact annotation on the object, guided by system-provided interactable ref-

\*Equal contribution.

†Corresponding author. Contact Information: Boran Wen, wenboran@sjtu.edu.cn; Ye Lu, Promaxultra@sjtu.edu.cn; Keyan Wan, xiyi38128@gmail.com; Sirui Wang, siruiwang@bjtu.edu.cn; Jiahong Zhou, zhoujiahong@sjtu.edu.cn; Junxuan Liang, whitefork@sjtu.edu.cn; Xinpeng Liu, xinpengliu0907@gmail.com; Bang Xiao, sherlockbang2005@gmail.com; Dingbang Huang, 13610214637@sjtu.edu.cn; Ruiyang Liu, liuruiyang@lincex.com; Yong-Lu Li, yonglu.li@sjtu.edu.cn.

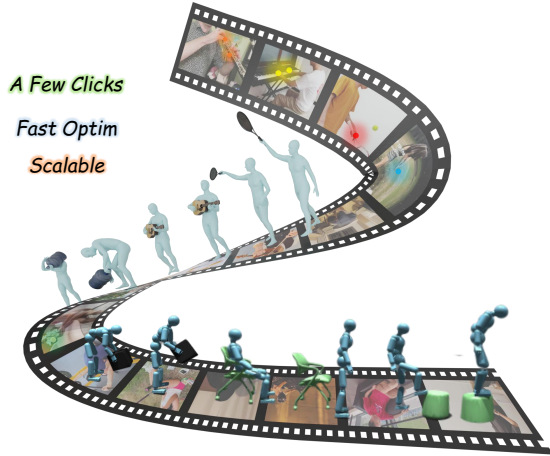


Figure 1. Our work aims to efficiently reconstruct HOI motions from in-the-wild monocular video data in an efficient and scalable manner, while enabling the reconstructed data to support downstream tasks such as humanoid learning and control.

reference points on the human body parts. Then, we develop *4DHOISolver*, a two-stage framework that first performs a rapid geometric alignment using least-squares matching and inverse kinematics, followed by a gradient-based optimization to refine the interaction’s physical plausibility. Leveraging this pipeline, we construct *Open4DHOI*, a diverse dataset containing 439 samples across 144 object categories and 103 actions, and develop a novel contact-based reward function to enable robust HOI motion imitation learning on the dataset. Overall, our work includes the following contributions:

- We propose *4DHOISolver*, a novel framework that reconstructs high-fidelity, physically plausible, and spatio-temporally coherent 4D HOI from monocular video by constraining a two-stage optimization with sparse contact point annotations.
- Leveraging this pipeline, we build and release *Open4DHOI*, a new, large-scale 4D HOI dataset.
- We demonstrate the effectiveness and utility of our dataset by developing a novel, contact-guided reward function and successfully training an RL-based agent to perform challenging HOI motion imitation.
- Our comprehensive benchmark of existing 3D large models reveals their significant limitations in predicting precise human-object correspondences, underscoring the necessity of our human-in-the-loop approach and posing an open challenge for future researches.

## 2. Related Works

### 2.1. 3D/4D HOI Datasets

Recently, many works [2, 6, 10, 25–27, 30, 31, 33, 35, 43] have focused on constructing 3D and 4D HOI datasets. Some works use multi-view RGB-D cameras to reconstruct

human SMPL [18] / SMPL-X [21] motion and object poses from depth point clouds and Mocap. BEHAVE [2] set up and calibrated 4 RGB-D cameras at four corners in a square recording volume, involving 8 subjects. InterCAP [25] followed BEHAVE by adding hand reconstruction and 2 cameras. Other works, such as HODome [27], used 76 RGB cameras for data capture, and *HOI – M<sup>3</sup>* [33] used 42 cameras. Other methods use Mocap suits for data collection, such as OMOMO [30], HUMOTO [26], and TRUMANS [31]. For object tracking, BEHAVE used fixed object keypoints to annotate positions in multi-view images manually, OMOMO and TRUMANS used markers, HUMOTO used two cameras, and FoundationPose [34] for tracking.

With the advancement of 3D reconstruction techniques, some recent works [6, 9, 35, 41, 43] have started to explore reconstructing human-object interaction data from monocular images and videos. Most of these works obtain human motion using state-of-the-art motion reconstruction tools, while object motion is handled with a variety of different approaches. WildHOI [43] constrains object pose by using pre-defined keypoints on object templates and adjusting their positions. Open3DHOI [35] reconstructs object meshes using state-of-the-art 3D reconstruction tools, followed by refinement in Blender. PICO [6] determines the object by matching the target image with similar meshes from a 3D object dataset [8] and applies contact constraints for further refinement.

### 2.2. 3D Reconstruction Tools

3D reconstruction tools provide foundations for reconstructing human-object interactions from monocular videos. First, human pose reconstruction tools [7, 13, 16, 24, 28] have become quite mature and can accurately estimate human poses in most scenarios. OSX [16] can simultaneously predict the body pose, hand pose, and facial expression of a person, but it lacks global information. GVHMR [7] can effectively reconstruct human motion in world space while ensuring alignment with the in-camera coordinate system and the input video, making it highly suitable for our project; however, it is unable to predict hand poses. HAMER [28] specializes in hand pose estimation, capable of accurately capturing hand details, which facilitates its integration with GVHMR for full-body pose estimation.

Secondly, 3D generative models [23, 36, 37] have made significant progress, especially in reconstructing target objects from single or multiple images, enabling the generation of high-quality meshes. These models are trained on large-scale 3D datasets like Objaverse [8], which can perform well on real images with high resolution now. In addition, image inpainting techniques [4, 20] can help address cases with partial occlusions. Pix2Gestalt [20] uses diffusion to predict the occluded parts of objects

from images, enabling simultaneous prediction of both the masked regions and the corresponding RGB information. Diffusion-VAS [4] can complete occluded parts of objects in videos while maintaining temporal consistency in the reconstructed regions.

### 3. Pipeline

In this section, we introduce how we efficiently collect and annotate in-the-wild, open-vocabulary HOI data, as well as perform fast reconstruction based on these annotations. Our core idea is to track key human-object contact “point pairs” and perform fast optimization-based reconstruction through point correspondence. Several important problems need to be addressed when using point-based annotation:

1) First, how to define keypoints for both the human body and the object. We address this by splitting the human body into several body parts and defining keypoints within each region as reference human interaction locations. Then, it only requires selecting the corresponding points on the object surface.

2) Second, how to constrain object pose with only point annotation. Previous works mostly optimize object pose through silhouette alignment. We directly optimize based on the annotation point pairs using mathematical methods, and we incorporate 2D point tracking to ensure the correctness of the object pose.

3) Third, how to ensure physical plausibility. We optimize the interactions using collision loss and smooth post-processing. In Sec. 4, our simulation result can also refine the reconstruction.

Specifically, in Sec. 3.1, we introduce a convenient and cost-free data collection approach. In Sec. 3.2, we obtain a coarse initialization reconstruction using existing 3D reconstruction techniques. Sec. 3.3 presents the annotation process and the working principles behind our annotation app. In Sec. 3.4, we describe how to achieve efficient and high-quality reconstruction from the annotated point pairs. Finally, in Sec. B, we introduce our constructed dataset Open4DHOI with various annotations and diversity.

#### 3.1. Data Collection

In-the-wild HOI 3D reconstruction requires data with high resolution, exo-centric, and easy accessibility — characteristics that short video data naturally possess. Based on this fact, we provide two data collection approaches. The first approach is to select clear, full-body videos from online platforms such as TikTok. The second approach is to record interaction videos using a mobile phone, while also capturing multi-view images of the object with the same phone. These multi-view object images are unobstructed and specifically intended for fine-grained object reconstruction.

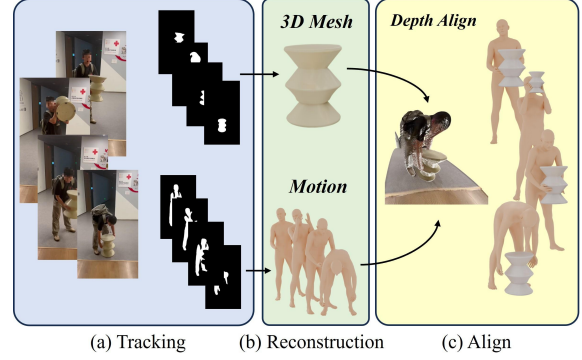


Figure 2. Our automated 4D reconstruction pipeline consists of three components: (a) human and object tracking, (b) 3D reconstruction, and (c) spatial alignment.

Each method has its pros and cons: TikTok videos feature more diverse scenes and richer interaction types, but have a higher failure rate in object reconstruction and require cleaning of non-interactive segments. In contrast, mobile phone recordings incur some manual labor costs but provide higher-quality data with controllable interaction actions.

#### 3.2. 4D Reconstruction

The quality of the initial 4D HOI reconstruction is significant for further annotation, which is highly dependent on the complexity of HOI motion and the quality of the input video. The main challenges are threefold: 1) In many cases, objects are heavily occluded, making reconstruction difficult. 2) In full-body interactions, accurately estimating the pose of each joint is challenging. 3) It is difficult to estimate the spatial relationship between the human and the object, as well as the size of the object.

To this end, we propose a complete 4D reconstruction pipeline shown in Fig. 2. Our proposed pipeline consists of the following stages:

1) Tracking both human and object masks using SAM2 [15]. For TikTok data, we also need to detect shot transitions and select the first frame containing human-object interaction as the starting point for subsequent reconstruction.

2) Next, we use image inpainting method [20] to complete the occluded object regions. Then we use TRELIS [36] for object reconstruction.

3) For human motion reconstruction, we employ GVHMR [7] for the full-body SMPL-X pose and HAMER [28] for fine-grained hand motion. The fused poses can ensure the plausibility of motion in most data.

4) Initializing and aligning the HOI poses through a depth-aware projection approach. Specifically, we estimate the depth of humans and objects based on DepthAnythingv2 [40] and use the depth point cloud for the spatial alignment and object scale estimation by projecting the hu-

man mesh and object mesh together to fit the point cloud.

### 3.3. Annotation App

#### 3.3.1. Contact Definition

A key prerequisite for annotating HOI point pairs is to define the interaction keypoints. Previous work predefined keypoints on object templates, which is not suitable for open-world object reconstruction. We choose to divide human joints as finely as possible while freely selecting the corresponding points on the object. We adopt a *tree structure* to define human keypoints, where 21 main body parts serve as parent nodes, and the child nodes represent finer subdivisions of each part, a total of **74** keypoints. For example, we divide the forearm into four points—front, back, left, and right—to ensure that contacts from all directions have corresponding interaction points.

#### 3.3.2. Annotation Procedure

To annotate HOI motion efficiently, we built an annotation app, as shown in Fig. 3. The user needs to annotate two parts. First, annotating the contact point pair between the object and the human body by selecting 3D point  $p_i^{3D}$  on the point cloud and the corresponding human joint  $q_i^{3D}$  in the joint tree. Second, constraining the object pose according to the video by annotating the 3D object point  $p_i^{2D}$  and clicking the corresponding 2D point  $q_i^{2D}$  on the frame.

Based on the fact that there are usually some fixed points in HOI motion, we aim to find and track these points, which makes the annotation process easy and fast. The user only needs to re-annotate when the stable points are changed in the video. Specifically, we use the Point Tracking model [14] to track the annotated 2D points. Interactive objects are divided into movable and static categories. For objects that remain motionless throughout the video, we provide an additional annotation option, allowing users to indicate whether the object pose should be fixed based on the video content. What’s more, for cases in Sec. 3.2 where the reconstructed object scale is inaccurate, we adjust the object’s scale before annotation.

### 3.4. 4DHOISolver

After obtaining the point annotations, we adopt a two-stage reconstruction approach called **4DHOISolver** in Fig. 4. In the first stage, we perform fast point-pair matching based on least squares and apply rapid inverse kinematics (IK) optimization to adjust the human limb positions. In the second stage, we refine the interaction’s physical plausibility through gradient-based optimization. This two-stage optimization framework ensures high efficiency while maintaining reconstruction accuracy.

#### 3.4.1. HOI Keypoint Solver

To achieve faster optimization while ensuring accuracy, we further designed a point matching method to align keypoint

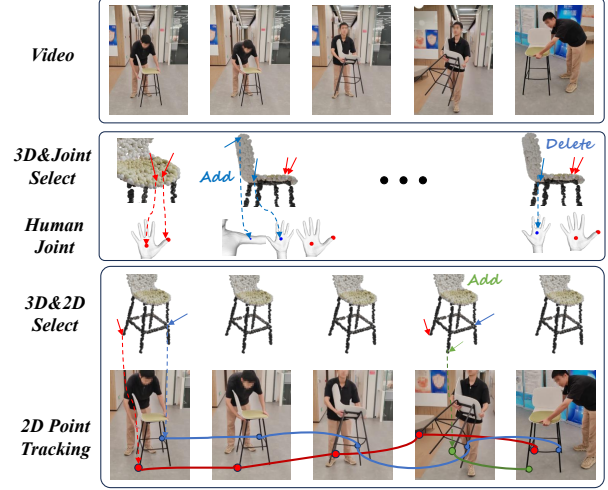


Figure 3. Annotation app: the first row shows the reference video, the second row displays the 3D-Human Joint annotations, and the third row presents the 3D-2D Projection annotations.

pairs and optimize the pose of the object. After completing the object pose optimization, we refine the human limb positions using IK.

Our core algorithm uses the least squares method to solve two Points-Alignment problem: 3D-3D spatial alignment and the 3D-2D projection alignment, as shown in Eq. 1, where the optimization targets are  $\mathbf{R}_o$  and  $\mathbf{t}_o$ .

$$\begin{aligned} \mathbf{r}_i^{3D}(\boldsymbol{\theta}) &= \sqrt{w_{3D}} (\mathbf{R}_o \mathbf{p}_i^{3D} + \mathbf{t}_o - \mathbf{q}_i^{3D}), \\ \mathbf{r}_j^{2D}(\boldsymbol{\theta}) &= \sqrt{w_{2D}} (\pi_{\mathbf{K}} (\mathbf{R}_o \mathbf{p}_j^{2D} + \mathbf{t}_o) - \mathbf{q}_j^{2D}), \\ \boldsymbol{\theta}^* &= \arg \min_{\boldsymbol{\theta}} \frac{1}{2} \left( \sum_{i=1}^N \|\mathbf{r}_i^{3D}(\boldsymbol{\theta})\|_2^2 + \sum_{j=1}^M \|\mathbf{r}_j^{2D}(\boldsymbol{\theta})\|_2^2 \right). \end{aligned} \quad (1)$$

By aligning the annotated point pairs, we can track the object’s pose and spatial position, as well as achieve coarse alignment of the contact regions. Since the limbs are the most critical parts for interaction and are prone to spatial misalignment, we apply a separate IK-based quick optimization specifically for the limbs.

#### 3.4.2. HOI Optimizer

**Optimization Goal.** Building on the initialization provided by the HOI solver, we propose an HOI optimizer to further refine the physical properties of Human–Object Interactions by optimizing  $\theta_h$ ,  $\mathbf{R}_o$ , and  $\mathbf{t}_o$ .

To make the optimization focus more on the annotated contact regions while maintaining stability in the non-contact areas, we propagate gradients only along the kinematic chain based on our joint-tree distances, ensuring that joints not directly involved in the optimization remain unaffected.

**Loss Function.** Our optimization process is driven by a composite loss function consisting of three terms: contact



---

**Algorithm 1** 4DHOISolver Optimization Pipeline

---

**Require:** Video frames with annotated 3D-3D and 3D-2D correspondences

- 1: Initialize model parameters (body pose, shape, object pose)
  - 2: **for** each frame  $t$  with step size 3 **do**
  - 3:   Perform weighted least squares optimization to estimate object pose ( $\mathbf{R}_t, \mathbf{t}_t$ ) using 3D-3D and 3D-2D correspondences
  - 4:   Run IK to refine human body pose parameters based on 3D keypoints
  - 5:   **for**  $i = 1$  to 20 **do**
  - 6:     Optimize body and object poses with collision, mask, and contact losses using the **Adam optimizer**
  - 7:   **end for**
  - 8:   **if**  $t > 0$  **then**
  - 9:     Interpolate parameters linearly between frames  $t - 3$  and  $t$
  - 10:   **end if**
  - 11: **end for**
  - 12: Apply low-pass filter smoothing on optimized poses across all frames
  - 13: **return** Optimized human and object poses
- 

loss, collision loss, and mask loss, as shown in Eq. 2.

$$L = w_c L_{\text{contact}} + w_{\text{coll}} L_{\text{collision}} + w_m L_{\text{mask}}. \quad (2)$$

$L$  address the limitation of HOI Keypoint Solver [11]’s point-based optimization, which ignores the physical plausibility of interaction, such as penetration, and allows for more fine-grained adjustments of the object’s pose estimation.

**Post-Smoothing.** To ensure optimization efficiency, we perform optimization every  $K$  frames and interpolate the intermediate frames, while applying a low-pass filter to smooth the entire optimized motion.

The overall optimization pipeline is as follows the Alg. 1.

### 3.5. Dataset

We collected a total of **439** sequences comprising **122k** frames across **144** categories of rigid objects through two ways: mobile-phone capture and TikTok crawling. Among them, **405** sequences (**107k** frames) were self-collected using mobile phones, and **34** sequences (**15k** frames) were crawled from TikTok.

It is worth noting that our data collection process is highly cost-efficient and requires no additional capture equipment. Our data annotation process takes approximately ten minutes per video and involves a simple, user-friendly workflow. In contrast, a single Azure Kinect RGB-D camera costs around \$399, while a complete Vicon motion capture system is priced at approximately \$50,000.

On average, each of our videos requires annotation of 6.7 points. Based on the Amazon Mechanical Turk (AMT) hourly wage, the cost curve is plotted in Fig. 6 (b). Meanwhile, we compare the costs and scales of Open3DHOI using Blender for frame-by-frame annotation with other 4D HOI datasets. It can be seen that our annotation method has strong scalability.

## 4. HOI Simulation

To demonstrate the scalability and easy-to-use property of our data, we adopt a test via humanoid body control. We train both the humanoid and the object in simulation with reinforcement learning. However, existing methods [19, 29, 32, 39] usually impose stringent requirements on the quality of the reference motion. As our reference motion is reconstructed from monocular videos with limited constraints, unreasonable reference HOI poses are sometimes inevitable under unseen or missing viewpoints, which affects the simulation results of current methods.

To this end, we developed a noise-robust, reference-less-reliable HOI simulation method based on InterMimic [39]. The goal of HOI simulation is to train a policy  $\pi$  that generates a physically plausible HOI motion sequence  $\{q_t^h, q_t^o\}_{t=1}^T$ . This sequence should be close to a reference motion sequence  $\{\hat{q}_t^h, \hat{q}_t^o\}_{t=1}^T$ , which is reconstructed by our 4DHOISolver.

The optimization target is defined as  $q_t^h = \{\theta_t^h, p_t^h\}$ , where  $\theta_t^h \in \mathbb{R}^{51 \times 3}$  represents the rotations of 52 human joints, and  $p_t^h$  denotes their positions. For the object,  $q_t^o = \{\theta_t^o, p_t^o\}$ , where  $\theta_t^o \in SO(3)$  is the object’s orientation and  $p_t^o \in \mathbb{R}^3$  is its position.

### 4.1. Tracking Reward

The tracking reward encourages the agent to imitate the reference pose. At each timestep  $t$ , given the simulated state  $s_t$  and reference state  $\hat{s}_t$ , we compute the reward based on the differences in joint positions  $p$ , angles  $\theta$ , velocities  $v$ , and angular velocities  $\omega$  for both the human and the object.

$$\begin{aligned} R_{\text{tr}} &= \exp \left( - (E_p^h + E_p^o + E_v^h + E_v^o) \right), \\ E_p^{h/o} &= \lambda_p \|\hat{p}_t^{h/o} - p_t^{h/o}\|^2 + \lambda_r \|\hat{\theta}_t^{h/o} \ominus \theta_t^{h/o}\|^2, \\ E_v^{h/o} &= \lambda_v \|\hat{v}_t^{h/o} - v_t^{h/o}\|^2 + \lambda_\omega \|\hat{\omega}_t^{h/o} - \omega_t^{h/o}\|^2, \end{aligned} \quad (3)$$

$\lambda_p, \lambda_r, \lambda_v, \lambda_\omega$  are the corresponding weights for each reward term, and  $\ominus$  calculates the difference in joint rotation.

### 4.2. KP Label Reward

To constrain the interaction regions, we further map the 74 predefined human keypoints from 4DHOISolver to the 52 joints of the humanoid model. We use the annotated keypoint pairs as GT contact labels and treat force feedback

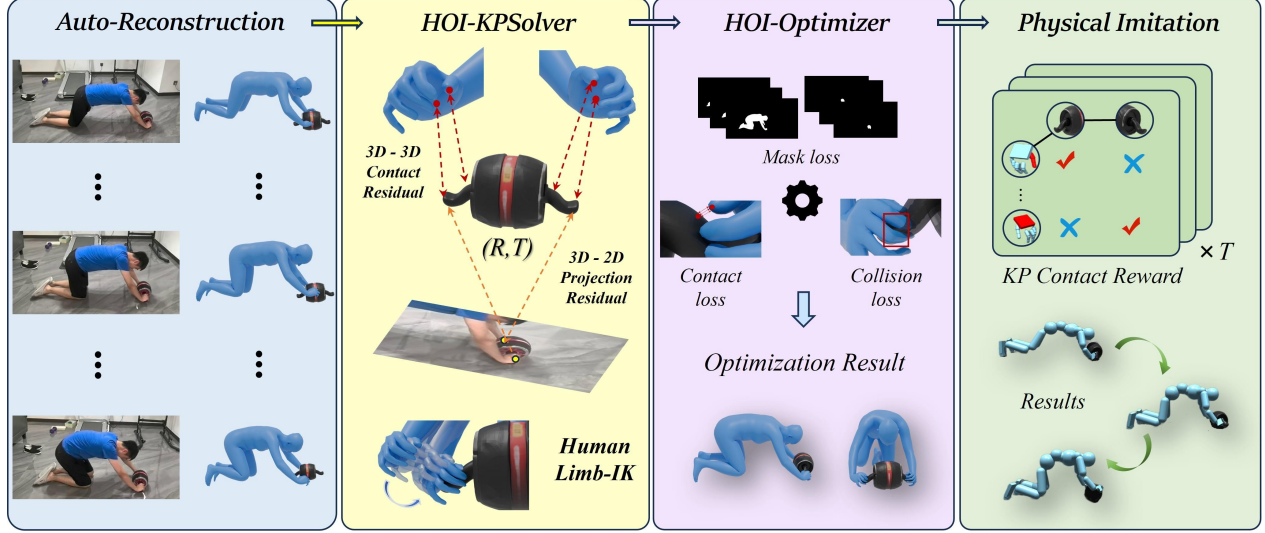


Figure 4. Pipeline: Our reconstruction pipeline consists of four stages. First, we perform automated reconstruction as described in Sec. 3.2. After obtaining the reconstructed results, we apply the 4DHOISolver from Sec. 3.4 for optimization based on the annotations. Finally, we conduct physical imitation as described in Sec. 4.

Table 1. HOI simulation results.

Reward	MPJPE (mm) ↓	contact (mm) ↓	jitter ↓
TR only	151.82	43.94	91.43
TR+LR	156.54	39.53	80.37
TR+LR+CR	<b>125.76</b>	<b>26.76</b>	<b>79.63</b>

as predicted contact labels during training, computing the corresponding discrepancies between them.

Specifically, the contact label reward is defined as:

$$R_{lr} = \sum \|\hat{c} - c\| \odot \hat{c}. \quad (4)$$

where  $\hat{c}$  is the reference contact label and  $c$  is the simulation contact label.

### 4.3. KP Contact Reward

To fully leverage our annotated point pairs and compensate for reconstruction inaccuracies, we designed a reward function based on 3D contact point pairs.

As shown in Fig. 4, we store all human-object point pair information in a contact table. In training, all annotated object points move along with the object, and at each corresponding frame, the distances between paired contact points are enforced to be zero according to the contact table. Specifically, We define all the annotated points of each motion object as  $M$ , and the interaction graph for each frame as  $I_g$ . The reward formula is given by:

$$R_{cr} = -\lambda_c \sum \|\theta_t^o M^o(I_g) + p_t^o - p_t^h(I_g)\|^2. \quad (5)$$

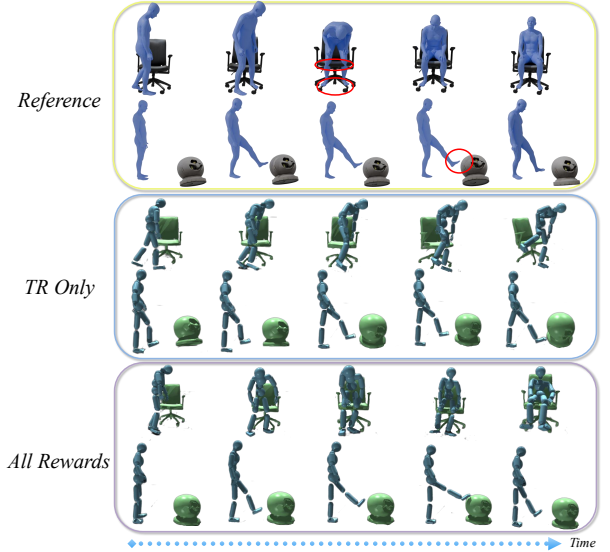


Figure 5. Visualization of our HOI Imitation results.

### 4.4. Optimization Results

To assess the performance of our method, we sample **80** sequences from Open4DHOI, containing a total of **29k** frames, and group them by action type. Each action is trained under three different reward settings. We evaluate the training results using three metrics: MPJPE (mean per joint position error) with reference motion, contact score, and jitter score to evaluate the smoothness of the motion. The results of the ablation study are summarized in Tab. 1. In Fig. 5, we visualize the imitation results of our method. It can be observed that our approach effectively optimizes physically implausible issues in the reference motion, such as interpenetration, foot floating, and contact misalignment.

Table 2. Dataset comparison across motion, object, and interaction diversity and quality.

Dataset	Quantity		Motion	Object			Interaction		Video	
	Frames	Sequences	Joint $\uparrow$	Category	Scale Range	Similarity $\uparrow$	Contact	Action	IS $\uparrow$	Scene
BEHAVE	15k	321	1.90	10	0.16 $\sim$ 0.82	1.143	Body	20	1.53	Indoor
OMOMO	810k	4.4k	1.57	15	0.24 $\sim$ 1.70	-	Body	34	-	Indoor
InterCap	67k	223	1.01	6	0.10 $\sim$ 0.69	0.830	Body+Hand	-	2.43	Indoor
PICO	4.1k	-	-	44	0.12 $\sim$ 3.21	0.808	Body+Hand	-	-	Wild
Open3DHOI	2.5k	-	-	133	0.02 $\sim$ 5.63	0.738	Body+Hand	120	-	Wild
Open4DHOI	122k	439	2.69	144	0.02 $\sim$ 4.22	0.870	Body+Hand	103	8.72	Wild

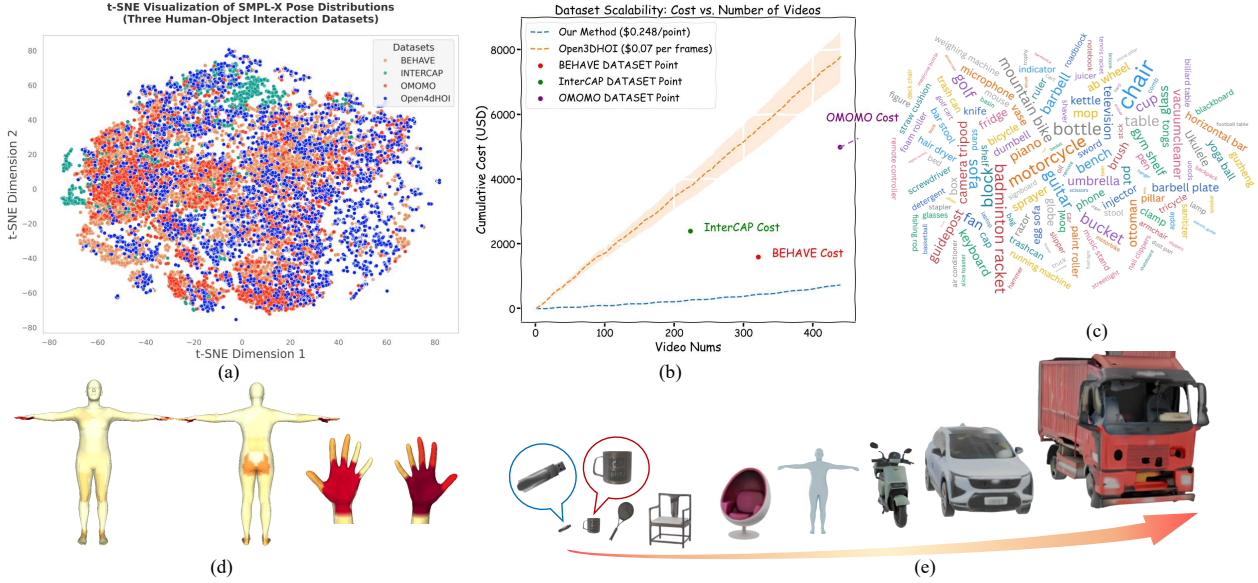


Figure 6. Dataset characteristics: (a) illustrates comparison of body pose diversity across different datasets, (b) shows that our dataset is easy to scale up, (c) presents a word cloud of the objects, (d) visualizes the distribution of annotated human contact label, and (e) depicts a scale-based visualization of the objects from smallest to largest.

## 5. Experiments

### 5.1. Dataset Experiments

#### 5.1.1. Diversity

Our dataset demonstrates high diversity across multiple dimensions. The objects exhibit a wide range of properties, encompassing various rigid bodies commonly found in everyday life. Human motions are equally diverse, involving movements that engage all major joints. Our dataset is also highly diverse at the interaction level, encompassing a wide range of actions as well as many uncommon HOIs.

**Object Diversity.** A key characteristic of our dataset is the rich variety of object categories. The objects span a wide range of sizes, as shown in the Tab. 2 and Fig. 6 (e).

**Motion Diversity.** The human body poses are more diverse compared to other video datasets. We visualized the top two principal components of SMPL-X body poses with t-SNE in Fig. 6 (a) and Tab. 2. It can be seen that the feature

points of our dataset encompass and cover those of the other three HOI video datasets.

**Interaction Diversity.** We used the Qwen2.5-vl-72B [1] model to annotate actions in the videos and further manually verified them. Ultimately, our dataset contains 103 object categories. For the BEHAVE and OMOMO datasets, we used Qwen2.5-72B [22] to extract action categories from the textual descriptions in the dataset and manually filtered the results. The outcomes are summarized in Tab. 2.

**Video Diversity.** To compare the scene diversity and variability of our video data, we evaluated it using the IS (Inception Score) metric. The results show that our dataset scores significantly higher than indoor datasets.

#### 5.1.2. Data Quality

We focused on evaluating the quality of object reconstruction and HOI motion optimization, demonstrating that our data can effectively support downstream tasks.

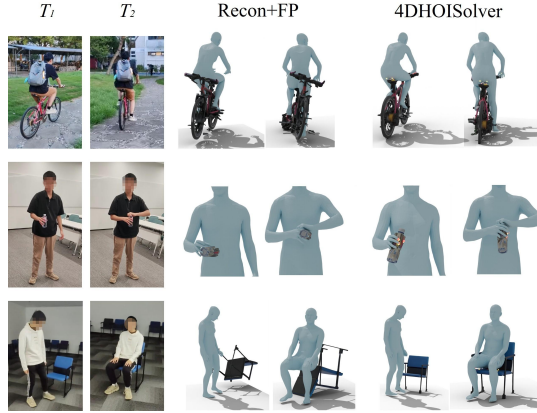


Figure 7. Visualized optimization results comparison between FoundationPose and 4DHOISolver.

Table 3. Reconstruction quality comparison.

Methods	collision $\uparrow$	contact (m) $\downarrow$	Proj (IoU) $\uparrow$
Recon	0.7090	0.439	0.6727
Recon+FP	0.7049	0.513	0.664
InteractVLM	0.7720	0.5561	0.612
Ours w/o Optim	0.7804	<b>0.1100</b>	0.702
Ours	<b>0.7865</b>	0.1105	<b>0.704</b>

**Reconstruction Quality.** We evaluated the quality of object reconstruction by comparing the similarity between the reconstructed objects and the images as the metric. We used OpenShape[17] to compare the feature similarity between meshes and their corresponding images, and the results in Tab. 2 show that our dataset outperforms other open-vocabulary datasets.

**Perceptual Evaluation.** To assess the reconstruction quality and contact point annotation accuracy of our dataset, we recruited five volunteers to rate all the data on a scale from 1 to 5. The results show strong performance, with 80% of the data scoring above 3.

## 5.2. HOI Motion Reconstruction

We evaluated the reconstruction performance of our 4DHOISolver against other baselines on the dataset, comparing several common metrics. These include the penetration score, which measures the degree of mesh interpenetration between humans and objects; the contact score, which assesses the distance between annotated contact points on humans and objects; and the projection score, which evaluates the IoU of the human and object reconstruction results projected onto the images.

The evaluated baselines include our automated reconstruction results (Recon), using FoundationPose for object pose estimation, and InteractVLM [9] with reconstruction performed every 10 frames. We also compared our method

Table 4. HOI contact prediction results evaluated across human, object, and interaction tasks.

Methods	Human	Object	HOI
LEMON	0.0636	0.2190	0.0164
InteractVLM	0.6012	0.2007	0.1204
PointLLM	0.4809	-	-
3D-AffordanceLLM	-	0.2220	-

without the HOI Optimizer refinement. The results in Tab. 3 demonstrate that our full method achieves the best optimization performance. Fig. 7 shows the visualization of our optimization results compared with FoundationPose.

## 6. HOI Contact Prediction

Our experiments validate the effectiveness of interaction point pairs for HOI reconstruction. However, existing 3D Models often focus on predicting contact regions for humans or objects separately, while overlooking explicit point-wise relationships. Given this, we evaluate four 3D models on our Open4DHOI dataset to test their abilities. The evaluation covers three tasks: human-side contact classification, object-side contact localization, and human-object contact point matching.

We test models including LEMON [41] and InteractVLM [9], which simultaneously predict human and object interaction regions; the 3D point cloud large model PointLLM [38]; and the LLM-based object affordance prediction model 3D-AffordanceLLM [5]. To reduce task difficulty, we use only the recall rate as the evaluation metric, measuring how much of the annotated contact region is correctly covered by each model’s predicted contact region. For 3D Q&A models like PointLLM, we input the merged point cloud of humans and objects optimized by 4DHOISolver, along with the object category, prompting the model to generate a textual description of the focused interaction human regions. We then use Qwen2.5-72B to extract the joint names from this description. The results in Tab. 4 show that existing 3D models still perform poorly in interaction prediction, especially when simultaneously predicting the correspondence between human and object interactions.

## 7. Discussion

Our method for reconstructing human interaction motions from monocular videos is efficient, but its accuracy depends on the capability of the underlying 3D reconstruction models. For instance, errors in hand reconstruction can severely affect the object’s pose, and the quality of object reconstruction ultimately determines whether the reconstruction data are successful. In the future, more powerful 3D reconstruction models will further reduce the difficulty and cost of our reconstruction process.



## 8. Conclusion

In conclusion, we present an efficient and scalable point-annotated pipeline to reconstruct 4D human–object interactions from open-world monocular videos. With the point-pair annotation, we built an optimization pipeline, 4DHOI-Solver, which is fast and accurate. To demonstrate that our reconstructed motion can be used for humanoid tasks, we designed an RL-based imitation pipeline. And we also tested existing 3D Models on our dataset for contact prediction ability, which shows the task remains challenging.

## Appendix Overview

The contents of this supplementary material are:

- Sec. A: Details of 4DHOISolver.
- Sec. B: Characteristics of Open4DHOI.
- Sec. C: Details of HOI Simulation.
- Sec. D: More Visualization Results.

## A. Details of 4DHOISolver

### A.1. Data Collection

To obtain high-quality HOI motions, the data must meet several requirements. First, clear and high-resolution video data are essential, as they are crucial for both object and human reconstruction.

Second, we require data that encompasses a wide variety of interactions and diverse scenes.

Third, we require full-body third-person view interaction data, as existing human reconstruction techniques still struggle to accurately estimate the poses of certain body parts.

We recruited volunteers to collect short video data from TikTok, requiring the clips to satisfy exo-centric viewpoints and full-body interactions. In addition, we adopted a two-person cooperative recording setup, where one volunteer captured the scene with a mobile phone while the other performed interactions with a designated object. We also required 1–4 multi-view images of the interacted object to be captured specifically for object reconstruction. These clear multi-view object images avoid occlusion issues and result in high-quality reconstructions. These two methods are shown in Fig. 8.

### A.2. Human Keypoint Definition

In Sec. 3.3.1, we mention that, for convenient and accurate interaction annotation, we predefine keypoints on the human body to serve as annotation targets. We first subdivide the human body parts by evenly splitting each major joint into front, back, left, and right regions. Then, for each subdivided part, we select a central point as the interaction keypoint. For the hand interaction points, we selected cor-

Table 5. Human joint-tree.

Main-Joints	Sub-Joints
leftForeArm	back, pinky, wrist, thumb
rightForeArm	back, pinky, wrist, thumb
leftUpperArm	up, down, back, front
rightUpperArm	up, down, back, front
leftShoulder	front, back
rightShoulder	front, back
leftHand	back, palm, Thumb, Index, Middle, Ring, Pinky
rightHand	back, palm, Thumb, Index, Middle, Ring, Pinky
leftUpperLeg	inner, outer, front, back
rightUpperLeg	inner, outer, front, back
leftLowerLeg	front, outer, back, inner
rightLowerLeg	front, outer, back, inner
leftFoot	ToeBase, instep, sole
rightFoot	ToeBase, instep, sole
upperSpine	back, right, front, left
middleSpine	front, right, back, left
leftNeck	front, back
rightNeck	back, front
hip	front, left, front, back
buttocks_left	buttocks_left
buttocks_right	buttocks_right

responding locations on all five fingers, as well as points on both the palm and the back of the hand.

In total, we defined 74 keypoints. Fig. 9 visualizes our human body keypoints, and Tab. 5 lists the names of the joints.



Figure 8. Data collection methods.

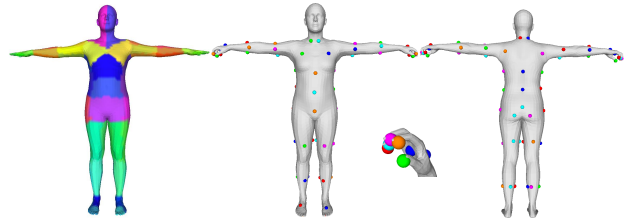


Figure 9. Human keypoint definition.

### A.3. Object Reconstruction

#### A.3.1. TikTok Reconstruction

In Sec. 3.2, we mention that for self-recorded data, object reconstruction is performed on multi-view images using TRELLIS to ensure high reconstruction quality. However, for TikTok-collected data, due to limited image completion capabilities, many cases with severe occlusions result in poor reconstruction quality. Therefore, we provide an alternative backup strategy.

We follow PICO’s object selection method by using OpenShape [17] from Objaverse to choose the most similar object, then compare its similarity score with the reconstructed object, selecting the higher one as the final object. This helps save bad reconstructions with TRELLIS due to severe occlusion.

#### A.3.2. Reconstruction Results

Fig. 10 shows the results of our object reconstruction. The first two rows display TikTok data after completion-based reconstruction: the skateboard in the first row was reconstructed using TRELLIS, while the motorcycle in the second row was retrieved from the Objaverse dataset. The last two rows show results from self-recorded data with multi-view object reconstruction. It can be seen that the objects captured by the phone without occlusion achieve very high reconstruction accuracy.

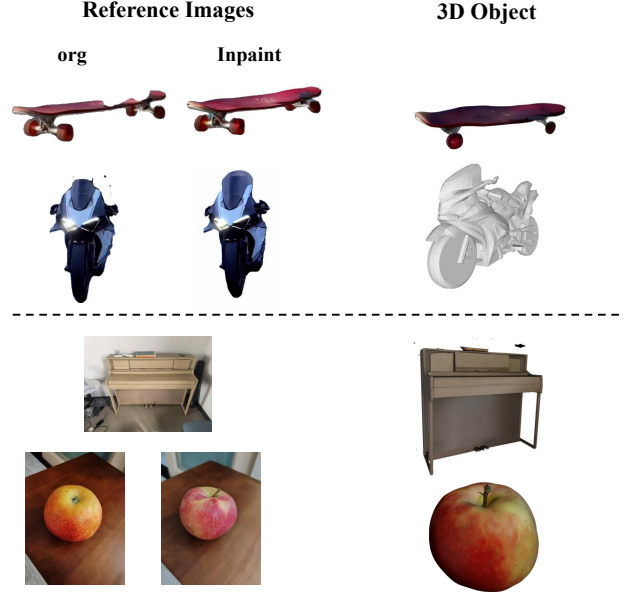


Figure 10. Visualizations of object reconstruction.

### A.4. Preprocess App

In Sec. 3.2, we mention that video tracking is required to obtain mask sequences of humans and objects for subsequent reconstruction. For TikTok videos, we identify the first frame where human-object interaction begins and manually annotate the masks of the human and object in that frame, providing point prompts for complete tracking using SAM2.

Fig. 11 illustrates our annotation workflow. We separately annotate prompt points for the human and object and display the segmentation results to ensure accurate subsequent tracking.

### A.5. Annotation App

Fig. 12 shows our annotation tool, which is used for labeling human-object contact point pairs and for 2D point tracking on objects. Our app mainly consists of a reference-video module, a 3D annotation module, and a human-keypoint annotation module. The following provides a detailed introduction to each of our annotation modules.

- **Video Display:** It displays the video to be annotated, allowing users to select specific frames for annotation by dragging the timeline or playing the video.
- **Check & Object Scale:** This module is used to inspect whether the automatically reconstructed object size from

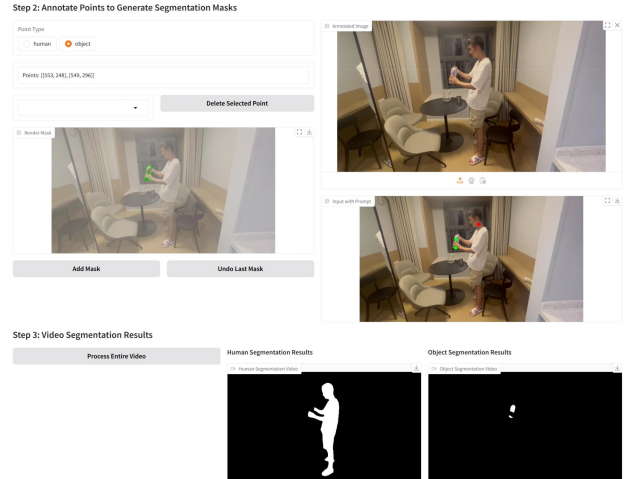


Figure 11. TikTok videos preprocessing for annotations.

Sec. 3.2 is correct, and to adjust the object scale when necessary.

- **Static Object:** We provide an option for annotators to mark an object as static when it remains stationary throughout the video. Once this option is selected, our subsequent optimization pipeline applies different strategies depending on whether the object is static or dynamic, enabling more efficient and stable processing.
- **Select 3D Points:** This module is used to select 3D contact points on the object, which are later matched with human keypoints or used for 2D point tracking. As shown in Fig. 13, the corresponding points are selected within the Open3D-based 3D visualization interface.

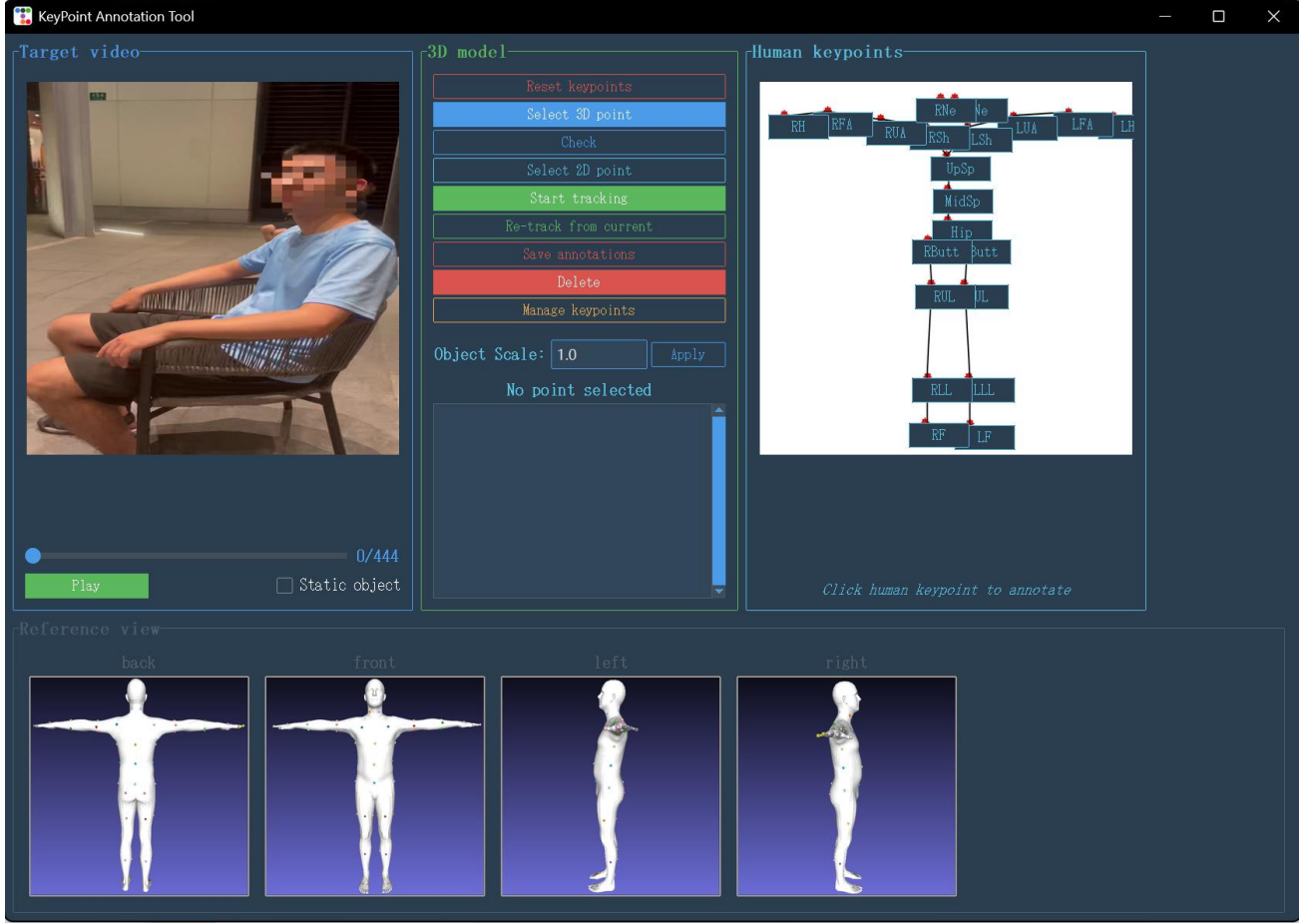


Figure 12. Annotation app.

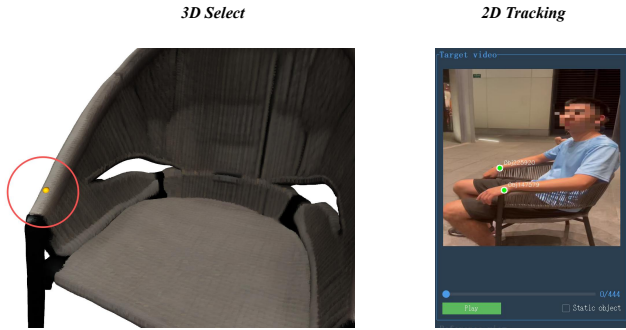


Figure 13. 3D annotation and 2D tracking annotation visualization.

- **Select 2D Point:** In this module, users select the projection of an object’s 3D point in the image of the current frame, which is used for tracking the object’s pose. To ensure tracking quality, we visualize the tracking results in the video and require annotators to correct the tracked points when necessary.

- **Manage Keypoints:** To speed up the annotation process, when some object points change contact positions during annotation, we only need to adjust the human joint or tracking positions without reselecting the object’s 3D points. At the same time, we allow deleting contact points that are no longer relevant while keeping the others intact, avoiding the need for re-annotation and greatly improving efficiency.
- **Human Keypoint:** We display the human interaction joints in a hierarchical joint tree on the right side of the app. Annotators can click a parent joint to expand its child nodes, and then click the corresponding child node to complete the annotation. Additionally, at the bottom of the app, we show the keypoint locations to help annotators easily find the most suitable contact points.

## A.6. Optimization

### A.6.1. Loss

In the HOI Optimizer, we use mask loss, contact loss, and collision loss for optimization. Here, we provide a detailed

explanation of how these loss functions are employed to enforce the physical plausibility of interactions.

**Mask Loss.** Let  $\hat{M}_h$ ,  $\hat{M}_o$ ,  $M_h$ , and  $M_o$  denote the rendered and ground-truth masks for the human and object, respectively. To handle mutual occlusions, we compute

$$\tilde{M}_h = \hat{M}_h(1 - M_o), \quad \tilde{M}_o = \hat{M}_o(1 - M_h). \quad (6)$$

We supervise the silhouettes with a pixel-wise MSE:

$$\mathcal{L}_{\text{mask}} = \text{MSE}(\tilde{M}_h, M_h) + \text{MSE}(\tilde{M}_o, M_o). \quad (7)$$

To enhance boundary accuracy, we extract edges via

$$E_h = \text{Pool}(\tilde{M}_h) - \tilde{M}_h, \quad E_o = \text{Pool}(\tilde{M}_o) - \tilde{M}_o, \quad (8)$$

and compute distance-transform weights  $W_h$ ,  $W_o$  on the ground-truth edges. The edge loss is

$$\mathcal{L}_{\text{edge}} = \sum E_h W_h + \sum E_o W_o. \quad (9)$$

The final loss is

$$\mathcal{L}_{\text{total}} = \alpha \mathcal{L}_{\text{mask}} + \beta \mathcal{L}_{\text{edge}}, \quad (10)$$

where  $\alpha$  and  $\beta$  are non-negative weights that balance the contributions of the mask and edge terms.

**Contact Loss.** Given corresponding human-object point pairs  $\{(p_i^h, p_i^o)\}_{i=1}^N$ , we compute their Euclidean distances for each pair as  $d_i = \|p_i^h - p_i^o\|_2$ . To encourage all pairs to converge to a globally balanced contact configuration, we assign larger weights to pairs with larger distances:

$$w_i = \frac{(d_i + \epsilon)^2}{\sum_{j=1}^N (d_j + \epsilon)^2}. \quad (11)$$

This weighting scheme pulls distant pairs more strongly while preventing near-contact pairs from dominating the gradients, leading to a uniform and stable convergence of all contact points.

The final contact loss is defined as:

$$\mathcal{L}_{\text{contact}} = \sum_{i=1}^N w_i d_i^2. \quad (12)$$

**Collision Loss.** To prevent interpenetration between the human mesh and the object mesh, we adopt the bidirectional mesh-to-mesh collision penalty used in [12]. Specifically, we apply the same collision operator to measure (i) human vertices inside the object surface and (ii) object vertices inside the human surface. The final collision loss is a weighted combination

$$\mathcal{L}_{\text{coll}} = \lambda_{h \rightarrow o} \mathcal{L}_{h \rightarrow o} + \mathcal{L}_{o \rightarrow h}, \quad (13)$$

where  $\lambda_{h \rightarrow o}$  controls the relative importance of penalizing human-inside-object penetration.

### A.6.2. Static Strategy

For videos labeled with the static-object option, we identify the frame with the largest number of annotated interaction points and use it as the static optimization frame. The object pose optimized in this frame is then fixed, and the object no longer participates in subsequent optimization steps. In the subsequent optimization process, only the human parameters are optimized.

## B. Characteristics of Open4DHOI

### B.1. Object Distribution

Our dataset contains a diverse and open-vocabulary range of object categories. To ensure that the collected data covers various real-life scenarios, we predefined 13 major categories and continuously expanded the object types within each category during data collection. Tab. 6 presents the statistics of video counts for each category, while Fig. 14 shows the specific objects included within each category.

### B.2. Action Annotation

In Sec. 5.1.1, we mention that we annotated 103 action categories for our dataset. We automatically extracted these action categories using a two-step strategy involving Qwen2.5-VL-72B [1] and Qwen2.5-72B-Instruct [22], followed by manual filtering.

First, we used Qwen2.5-VL-72B to extract interaction descriptions from the videos. The prompt we provided was: “There exists human and {obj\_name} in the video. Please describe the interactions between the person and the object completely and accurately. Output full sentences.”

Next, we used Qwen2.5-72B-Instruct to extract the action categories. We adopted the action list from HICO-DE [3] as a pool of candidate actions and prompted the model to select the actions present in each video from this list. The prompt we provided was: “Here is a human-{obj\_name} action description: {interaction\_description}. Please select the most similar human-{obj\_name} interaction action from the following candidate list.”

### B.3. Co-occurrence of HOI

We plotted the co-occurrence matrix between actions and object categories, as shown in Fig. 15. It can be observed that our dataset contains many hand-related interaction objects, including actions such as “pick up” and “hold”, as well as frequent interactions “like sit” and “stand on”. This also demonstrates that our dataset covers a highly diverse range of HOI categories.



Table 6. Major categories counts.

Major Categories	Value
daily use	104
vehicles	80
furniture	51
sports	48
tools	46
instruments	28
electronics	24
kitchen	18
infrastructure	17
stationary	13
clothing	5
weapon	3
fruit	2

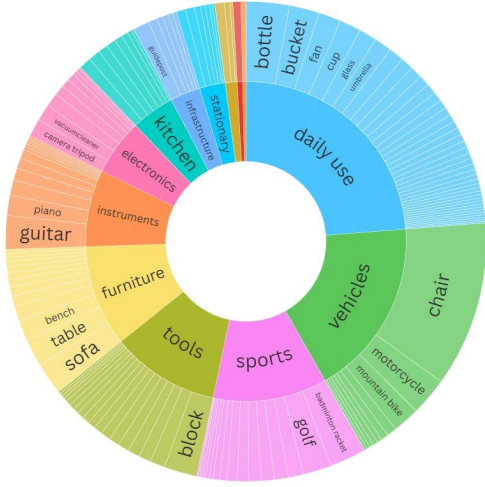


Figure 14. Object distribution.

## C. Details of HOI Simulation

### C.1. Implementation Details

The reference data is derived from human bodies represented using SMPL-X [21]. For simulation, we retarget these models into rigid bodies following [19, 42], and Objects are also converted into simulation models through convex decomposition. Similar to existing methods [29, 39], we perform HOI-simulation in Isaac Gym and use the first reference frame to initialize the simulation environment. The parameter settings for simulation environments are shown in the Tab. 7 To distinguish between static and dynamic objects derived from the annotation information, we set different physical mass for them. This ensures physical plausibility while satisfying the static object constraint as much as possible.

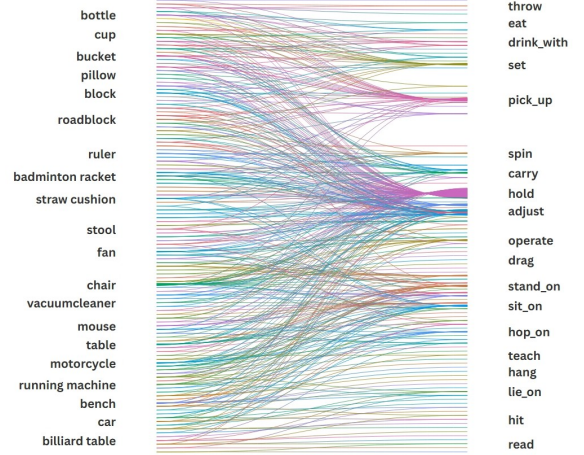


Figure 15. Co-occurrence between object categories and actions in Open4DHOI.

Table 7. Simulation hyperparameters.

Hyperparameter	Value
Sim dt	1/60s
Control dt	1/30s
Number of envs	1024
Number of substeps	4
Number of pos iterations	8
Number of vel iterations	1
Contact offset	0.2
Rest offset	0.0
Max depenetration velocity	20
Object friction	0.6
Object static mass	10000
Object dynamic mass	0.5
Object & ground restitution	0.05 / 0.1
Object density	1000
Object max convex hulls	64

### C.2. Metrics

As described in the Sec. 4, we divided 80 sequences into 12 subsets by action type and trained one policy per subset. To validate our method, we tested and computed three metrics: MPJPE, contact score, and jitter. In this section, we provide further details about how these metrics are calculated. MPJPE (Mean Per Joint Position Error) is used to measure the average distance between the skeleton joint positions in simulation and the reference joint positions. It directly reflects the overall accuracy of pose or trajectory reconstruction. A smaller value indicates more accurate reconstruction.

$$\text{MPJPE} = \frac{1}{T|\mathcal{J}|} \sum_{t=1}^T \sum_{j=1}^{\mathcal{J}} \|\hat{p}_{t,j}^h - p_{t,j}^h\|_2, \quad (14)$$

where  $T$  denotes the total number of frames,  $\mathcal{J}$  represents the set of human joints, and  $|\mathcal{J}|$  indicates its cardinality.

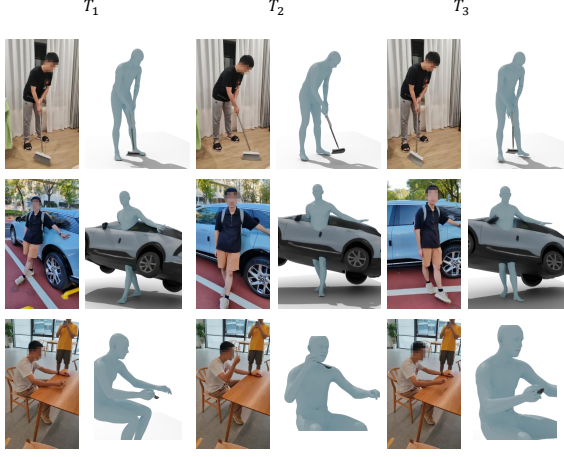


Figure 16. Failure cases of 4DHOISolver reconstruction.

The term  $\hat{p}_{t,j}^h$  refers to the simulated 3D position of joint  $j$  at frame  $t$ , while  $p_{t,j}^h$  denotes the corresponding ground-truth joint position.

The contact score is computed as the sum of squared Euclidean distances between each pair of annotated keypoints in the interaction graph  $I_g$ . During retargeting, the SMPL-X keypoints that we annotated are converted into positions of skeleton joints. This score is used to check whether the newly added reward successfully improves the contact relationships during simulation.

$$\text{Contact} = \sum \|\theta_t^o M^o(I_g) + p_t^o - p_t^h(I_g)\|^2, \quad (15)$$

where  $\theta_t^o$  and  $p_t^o$  represent the object’s rotation and translation at frame  $t$ ,  $M^o(I_g)$  selects the object keypoints defined by the interaction graph  $I_g$ , and  $p_t^h(I_g)$  denotes the corresponding human joint positions.

The jitter score is used to measure the smoothness and stability of a sequence over time, and indicates whether noticeable jitter is present. A lower value indicates smoother, more coherent motion. The calculation is as follows:

$$\text{Jitter} = \frac{1}{|\mathcal{J}|} \sum_{j \in \mathcal{J}} \sqrt{\frac{1}{T-3} \sum_t \|\Delta^3 \mathbf{p}_{t,j}^h\|^2}. \quad (16)$$

## D. More Visualization Results

### D.1. Failure Cases

Fig. 16 presents several failure cases of our reconstruction results. The first row shows cases where inaccurate object scale leads to incorrect contact. The second row illustrates failures caused by inaccurate 2D keypoint annotations, resulting in incorrect object poses. The third row shows examples where severe occlusion makes the 2D keypoints difficult to track, and relying solely on 3D constraints is insufficient for accurate reconstruction.

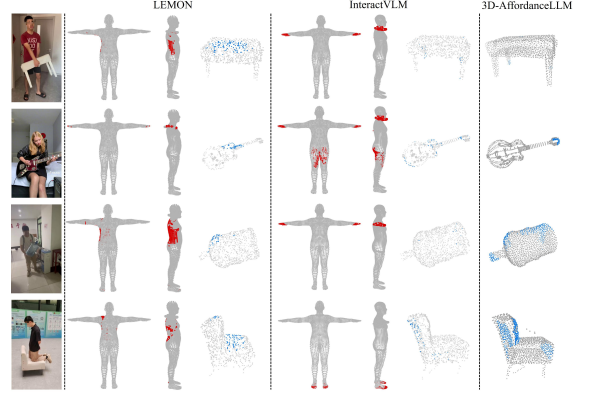


Figure 17. Visual comparison of HOI contact predictions.

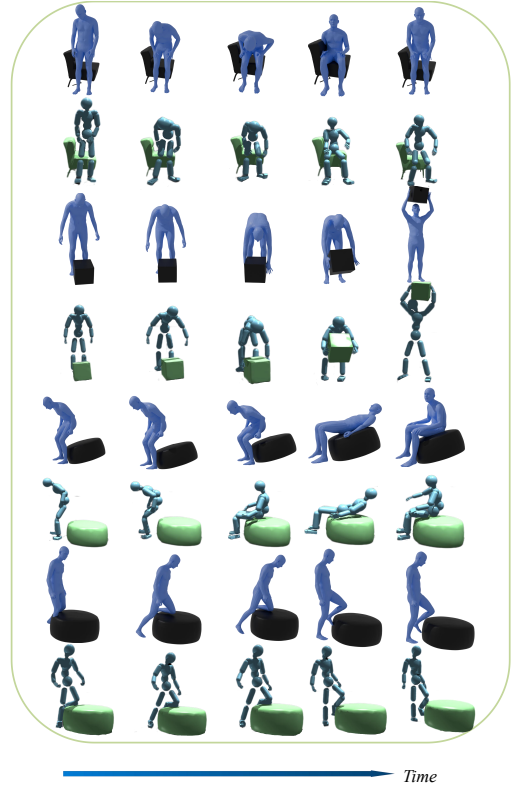


Figure 18. Qualitative results of the HOI simulation.

### D.2. HOI Contact Prediction

In Fig. 17, we show contact area prediction results of three 3D Models.

### D.3. HOI Simulation

In this section, we provide additional visualizations from the HOI-simulation, shown in Fig. 18.

### D.4. Reconstruction

Fig. 19 shows more visualization results of our 4DHOISolver reconstructions.

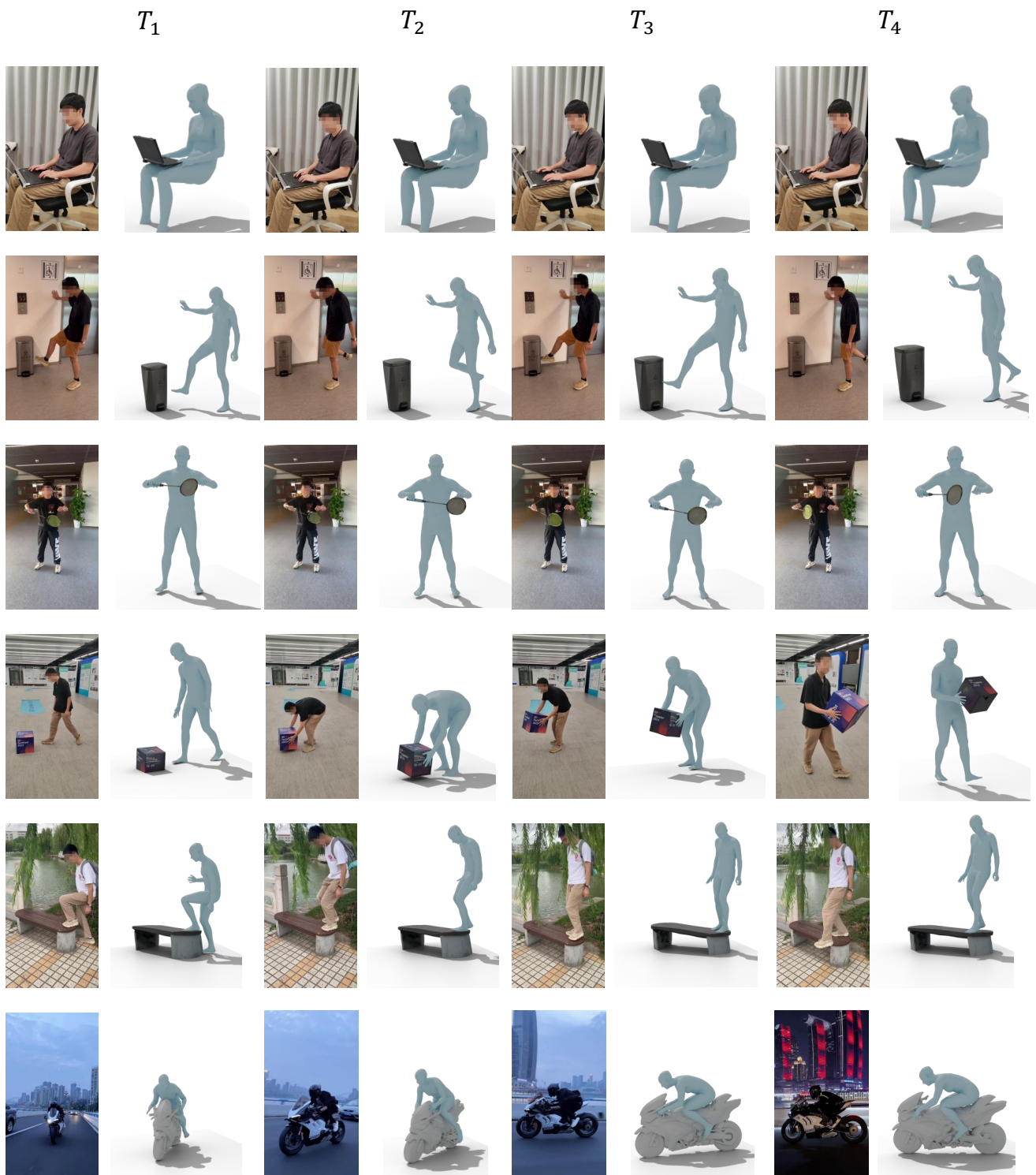


Figure 19. More visualization of 4DHOISolver reconstructions.

## References

- [1] Shuai Bai, Keqin Chen, Xuejing Liu, Jialin Wang, Wenbin Ge, Sibao Song, Kai Dang, Peng Wang, Shijie Wang, Jun

Tang, Humen Zhong, Yuanzhi Zhu, Mingkun Yang, Zhao-hai Li, Jianqiang Wan, Pengfei Wang, Wei Ding, Zheren



- Fu, Yiheng Xu, Jiabo Ye, Xi Zhang, Tianbao Xie, Zesen Cheng, Hang Zhang, Zhibo Yang, Haiyang Xu, and Junyang Lin. Qwen2.5-vl technical report. *arXiv preprint arXiv:2502.13923*, 2025. 7, 12
- [2] Bharat Lal Bhatnagar, Xianghui Xie, Ilya Petrov, Cristian Sminchisescu, Christian Theobalt, and Gerard Pons-Moll. Behave: Dataset and method for tracking human object interactions. In *IEEE Conference on Computer Vision and Pattern Recognition (CVPR)*. IEEE, 2022. 1, 2
- [3] Yu-Wei Chao, Yunfan Liu, Xieyang Liu, Huayi Zeng, and Jia Deng. Learning to detect human-object interactions. In *Proceedings of the IEEE Winter Conference on Applications of Computer Vision*, 2018. 12
- [4] Kaihua Chen, Deva Ramanan, and Tarasha Khurana. Using diffusion priors for video amodal segmentation, 2024. 2, 3
- [5] Hengshuo Chu, Xiang Deng, Qi Lv, Xiaoyang Chen, Yinchuan Li, Jianye Hao, and Liqiang Nie. 3d-affordancellm: Harnessing large language models for open-vocabulary affordance detection in 3d worlds. In *Proceedings of the International Conference on Learning Representations (ICLR)*, 2025. 8
- [6] Alpár Cseke, Shashank Tripathi, Sai Kumar Dwivedi, Arjun Lakshmipathy, Agniv Chatterjee, Michael J. Black, and Dimitrios Tzionas. PICO: Reconstructing 3D people in contact with objects. In *Proceedings of the IEEE/CVF Conference on Computer Vision and Pattern Recognition (CVPR)*, pages 1783–1794, 2025. 1, 2
- [7] Yudi Dai, Yubin Hu, Gengshan Yang, Deqing Sun, and Xiaolong Wang. Gvhmr: Generative human-object motion reconstruction in a generative world model. *arXiv preprint arXiv:2411.17981*, 2024. 2, 3
- [8] Matt Deitke, Ruoshi Liu, Matthew Wallingford, Huong Ngo, Oscar Michel, Aditya Kusupati, Alan Fan, Christian Laforte, Vikram Voleti, Samir Yitzhak Gadre, Eli VanderBilt, Aniruddha Kembhavi, Carl Vondrick, Georgia Gkioxari, Kiana Ehsani, Ludwig Schmidt, and Ali Farhadi. Objaverse-xl: A universe of 10m+ 3d objects. *arXiv preprint arXiv:2307.05663*, 2023. 2
- [9] Sai Kumar Dwivedi, Dimitrije Antić, Shashank Tripathi, Omid Taheri, Cordelia Schmid, Michael J. Black, and Dimitrios Tzionas. Interactvlm: 3d interaction reasoning from 2d foundational models, 2025. 2, 8
- [10] Mohamed Hassan, Vasileios Choutas, Dimitrios Tzionas, and Michael J. Black. Resolving 3D human pose ambiguities with 3D scene constraints. In *International Conference on Computer Vision*, 2019. 2
- [11] Yana Hasson, Bugra Tekin, Federica Bogo, Ivan Laptev, Marc Pollefeys, and Cordelia Schmid. Leveraging photometric consistency over time for sparsely supervised hand-object reconstruction, 2020. 5
- [12] Wen Jiang, Nikos Kolotouros, Georgios Pavlakos, Xiaowei Zhou, and Kostas Daniilidis. Coherent reconstruction of multiple humans from a single image. In *CVPR*, 2020. 12
- [13] Angjoo Kanazawa, Jason Y. Zhang, Panna Felsen, and Jitendra Malik. Learning 3d human dynamics from video. In *Computer Vision and Pattern Recognition (CVPR)*, 2019. 2
- [14] Nikita Karaev, Ignacio Rocco, Benjamin Graham, Natalia Neverova, Andrea Vedaldi, and Christian Rupprecht. Co-tracker: It is better to track together. In *Proc. ECCV*, 2024. 4
- [15] Nikita Karaev, Ignacio Rocco, Benjamin Graham, Natalia Neverova, Andrea Vedaldi, and Christian Rupprecht. Sam2: Segment anything in images and videos. *arXiv preprint arXiv:2409.00779*, 2024. 3
- [16] Jing Lin, Ailing Zeng, Haoqian Wang, Lei Zhang, and Yu Li. One-stage 3d whole-body mesh recovery with component aware transformer. In *Proceedings of the IEEE/CVF Conference on Computer Vision and Pattern Recognition*, pages 21159–21168, 2023. 2
- [17] Minghua Liu, Ruoxi Shi, Kaiming Kuang, Yinhao Zhu, Xuanlin Li, Shizhong Han, Hong Cai, Fatih Porikli, and Hao Su. Openshape: Scaling up 3d shape representation towards open-world understanding, 2023. 8, 10
- [18] Matthew Loper, Naureen Mahmood, Javier Romero, Gerard Pons-Moll, and Michael J. Black. *SMPL: A Skinned Multi-Person Linear Model*. Association for Computing Machinery, New York, NY, USA, 1 edition, 2023. 2
- [19] Zhengyi Luo, Jinkun Cao, Alexander W. Winkler, Kris Kitani, and Weipeng Xu. Perpetual humanoid control for real-time simulated avatars. In *International Conference on Computer Vision (ICCV)*, 2023. 5, 13
- [20] Ege Ozguroglu, Ruoshi Liu, Dídac Surís, Dian Chen, Achal Dave, Pavel Tokmakov, and Carl Vondrick. pix2gestalt: Amodal segmentation by synthesizing wholes. *Proceedings of the IEEE/CVF Conference on Computer Vision and Pattern Recognition (CVPR)*, 2024. 2, 3
- [21] Georgios Pavlakos, Vasileios Choutas, Nima Ghorbani, Timo Bolkart, Ahmed A. A. Osman, Dimitrios Tzionas, and Michael J. Black. Expressive body capture: 3D hands, face, and body from a single image. In *Proceedings IEEE Conf. on Computer Vision and Pattern Recognition (CVPR)*, pages 10975–10985, 2019. 2, 13
- [22] Qwen, :, An Yang, Baosong Yang, Beichen Zhang, Binyuan Hui, Bo Zheng, Bowen Yu, Chengyuan Li, Dayiheng Liu, Fei Huang, Haoran Wei, Huan Lin, Jian Yang, Jianhong Tu, Jianwei Zhang, Jianxin Yang, Jiayi Yang, Jingren Zhou, Junyang Lin, Kai Dang, Keming Lu, Keqin Bao, Kexin Yang, Le Yu, Mei Li, Mingfeng Xue, Pei Zhang, Qin Zhu, Rui Men, Runji Lin, Tianhao Li, Tianyi Tang, Tingyu Xia, Xingzhang Ren, Xuancheng Ren, Yang Fan, Yang Su, Yichang Zhang, Yu Wan, Yuqiong Liu, Zeyu Cui, Zhenru Zhang, and Zihan Qiu. Qwen2.5 technical report, 2025. 7, 12
- [23] Ruoxi Shi, Hansheng Chen, Zhuoyang Zhang, Minghua Liu, Chao Xu, Xinyue Wei, Linghao Chen, Chong Zeng, and Hao Su. Zero123++: a single image to consistent multi-view diffusion base model, 2023. 2
- [24] Qingping Sun, Yanjun Wang, Ailing Zeng, Wanqi Yin, Chen Wei, Wenjia Wang, Haiyi Mei, Chi Sing Leung, Ziwei Liu, Lei Yang, and Zhongang Cai. Aios: All-in-one-stage expressive human pose and shape estimation, 2024. 2
- [25] Garvita Tiwari, Dimitrije Antic, Jan T. Erbach, Michael A. W. Li, Tim Lüddecke, Aljoša Ošep, Juergen Gall, and Bastian Leibe. Intercap: Joint markerless 3d tracking of humans and objects in interaction from multi-view data. In



- 2022 *International Conference on 3D Vision (3DV)*, pages –. IEEE, 2022. [2](#)
- [26] Ziniu Wan, Yichen Wang, Yuchong Sun, and Song Bai. Humoto: A unified model for 3d human motion and object tracking. In *Advances in Neural Information Processing Systems*, pages –, 2023. [2](#)
- [27] Ziniu Wan, Yuchong Sun, Zhening Huang, Pheng-Ann Heng, and Song Bai. Hodome: A 3d indoor dataset for holistic human-object interaction detection. In *Proceedings of the ACM on Multimedia Conference*, 2024. [2](#)
- [28] Tianyu Wang, Yuxiao Chen, Liangyan Gui, Longwei Guo, Jianfeng Zhang, Yujun Cai, and Yandong Guo. Hamer: 3d hand and body mesh recovery from a single image with hierarchical attention. *arXiv preprint arXiv:2411.17492*, 2024. [2](#), [3](#)
- [29] Yinhuai Wang, Jing Lin, Ailing Zeng, Zhengyi Luo, Jian Zhang, and Lei Zhang. Physshoi: Physics-based imitation of dynamic human-object interaction, 2023. [5](#), [13](#)
- [30] Yichen Wang, Ziniu Wan, Yuchong Sun, and Song Bai. Omomo: A one-stage model for open-vocabulary human-object interaction detection via multi-view supervision. In *Proceedings of the IEEE/CVF International Conference on Computer Vision*, pages –, 2023. [2](#)
- [31] Yichen Wang, Ziniu Wan, Yuchong Sun, and Song Bai. Trumans: A task and domain-aware model for human-object interaction detection. In *Proceedings of the AAAI Conference on Artificial Intelligence*, pages –, 2024. [2](#)
- [32] Yinhuai Wang, Qihan Zhao, Runyi Yu, Hok Wai Tsui, Ailing Zeng, Jing Lin, Zhengyi Luo, Jiwen Yu, Xiu Li, Qifeng Chen, Jian Zhang, Lei Zhang, and Ping Tan. Skillmimic: Learning basketball interaction skills from demonstrations. In *Proceedings of the Computer Vision and Pattern Recognition Conference (CVPR)*, pages 17540–17549, 2025. [5](#)
- [33] Yani Wei, Zeyu Zhang, Hongchen Luo, Yanjun Wang, Di Huang, Junyu Dong, and Hengshuang Zhao. Hoi-m<sup>3</sup>: A large-scale 3d multi-multi-view multi-object multi-human dataset for human-object interaction. In *Advances in Neural Information Processing Systems*, 2024. [2](#)
- [34] Bowen Wen, Wei Yang, Jan Kautz, and Stan Birchfield. Foundationpose: A unified foundation model for object pose estimation. *arXiv preprint arXiv:2402.17427*, 2024. [2](#)
- [35] Boran Wen, Dingbang Huang, Zichen Zhang, Jiahong Zhou, Jianbin Deng, Jingyu Gong, Yulong Chen, Lizhuang Ma, and Yong-Lu Li. Reconstructing in-the-wild open-vocabulary human-object interactions, 2025. [1](#), [2](#)
- [36] Yufei Xie, Sachith Seneviratne, Sanjay Haresh Seneviratne, Alex Schwing, Junyi Geng, and Huazhe Xu. Trellis: Human-aware object placement via trajectory likelihoods in space. In *Proceedings of the IEEE/CVF Conference on Computer Vision and Pattern Recognition*, pages 17978–17988, 2024. [2](#), [3](#)
- [37] Jiale Xu, Weihao Cheng, Yiming Gao, Xintao Wang, Shenghua Gao, and Ying Shan. Instantmesh: Efficient 3d mesh generation from a single image with sparse-view large reconstruction models, 2024. [2](#)
- [38] Runsen Xu, Xiaolong Wang, Tai Wang, Yilun Chen, Jiangmiao Pang, and Dahua Lin. Pointllm: Empowering large language models to understand point clouds. In *ECCV*, 2024. [8](#)
- [39] Sirui Xu, Hung Yu Ling, Yu-Xiong Wang, and Liang-Yan Gui. InterMimic: Towards universal whole-body control for physics-based human-object interactions. In *CVPR*, 2025. [5](#), [13](#)
- [40] Lihe Yang, Bingyi Kang, Zilong Huang, Zhen Zhao, Xiaogang Xu, Jiashi Feng, and Hengshuang Zhao. Depth anything v2. *arXiv:2406.09414*, 2024. [3](#)
- [41] Yuhang Yang, Wei Zhai, Hongchen Luo, Yang Cao, and Zheng-Jun Zha. Lemon: Learning 3d human-object interaction relation from 2d images. *arXiv preprint arXiv:2312.08963*, 2023. [2](#), [8](#)
- [42] Ye Yuan, Shih-En Wei, Tomas Simon, Kris Kitani, and Jason Saragih. Simpo: Simulated character control for 3d human pose estimation, 2021. [13](#)
- [43] Zeyu Zhang, Yani Wei, Hongchen Luo, Di Huang, Yanjun Wang, Junyu Dong, and Hengshuang Zhao. Wildhoi: Boosting category-level human-object interaction detection in the wild with large-vocabulary dataset. *arXiv preprint arXiv:2410.12128*, 2024. [2](#)